Analyst



PAPER View Article Online View Journal



Cite this: DOI: 10.1039/d4an00393d

Combined electrical-electrochemical phenotypic profiling of antibiotic susceptibility of *in vitro* biofilm models†

Zahra Rafiee, Maryam Rezaie and Seokheun Choi ** **a,b

More than 65% of bacterial infections are caused by biofilms. However, standard biofilm susceptibility tests are not available for clinical use. All conventional biofilm models suffer from a long formation time and fail to mimic in vivo microbial biofilm conditions. Moreover, biofilms make it difficult to monitor the effectiveness of antibiotics. This work creates a powerful yet simple method to form a target biofilm and develops an innovative approach to monitoring the antibiotic's efficacy against a biofilm-associated infection. A paper-based culture platform can provide a new strategy for rapid microbial biofilm formation through capillary action. A combined electrical-electrochemical technique monitors bacterial metabolism rapidly and reliably by measuring microbial extracellular electron transfer (EET) and using electrochemical impedance spectroscopy (EIS) across a microbe-electrode interface. Three representative pathogens, Pseudomonas aeruginosa, Escherichia coli, and Staphylococcus aureus, form their biofilms controllably within an hour. Within another hour their susceptibilities to three frontline antibiotics with different action modes (gentamicin, ciprofloxacin, and ceftazidime) are examined. Our antibiotic susceptibility testing (AST) technique provides a quantifiable minimum inhibitory concentration (MIC) of those antibiotics against the *in vitro* biofilm models and characterizes their action mechanisms. The results will have an important positive effect because they provide immediately actionable healthcare information at a reduced cost, revolutionizing public healthcare.

Received 13th March 2024, Accepted 22nd April 2024 DOI: 10.1039/d4an00393d

rsc.li/analyst

1. Introduction

Distinct bacteria in nature can be in close proximity by forming biofilms with or without adhering to a surface. In this way, bacteria can survive and adapt to new environments, facilitate their growth and proliferation, and enhance protection from environmental dangers. Within biofilms, bacteria can alter their genotypes and phenotypes, rearrange their spatial structures, and regulate their cooperative activities, developing unique community-intrinsic properties that are not observed in counterparts growing planktonically. Because of these functional updates, however, biofilms are often detrimental, posing serious concerns to human health, water distribution systems, food and groceries, and industrial productivity. Usually, bacteria densely packed in biofilms enhance virulence factors and

Reliable models that mimic complex and diverse biofilms are essential to have an in-depth understanding of the biofilm properties and improve the ability to remove biofilms. ¹⁶ Unfortunately, although diverse models of biofilm formation have been developed for the past several decades, there are no universally standardized models for the simple, rapid, reliable, and effective formation and development of biofilms. ^{11,14,16} Animal models have recently received significant attention because they resemble *in vivo* biofilms and represent 3-D

become more infectious than planktonic cells.⁸ Moreover, their presence in a biofilm considerably increases bacteria's resistance to antibiotics, turning infections more severe and making treatment more difficult.^{9,10} The infections ultimately require surgery or the replacement of implanted materials to eradicate the biofilm.¹¹ Those biofilm-associated infections are estimated to cause more than 500 000 death per year in the United States and cost more than \$100 billion annually.¹² Moreover, misuse and overuse of broad-spectrum antibiotics have promoted the development of antibiotic resistance, leading to life-threatening infections, and growing treatment resistance.¹³ Most conventional *in vitro* biofilm models fail to mimic human *in vivo* microbial biofilms.¹⁴ Moreover, conventional monitoring techniques such as antibiotic susceptibility testing (AST) are limited to planktonic bacteria.¹⁵

^aBioelectronics & Microsystems Laboratory, Department of Electrical & Computer Engineering, State University of New York at Binghamton, Binghamton, New York, 13902, USA. E-mail: sechoi@binghamton.edu

^bCenter for Research in Advanced Sensing Technologies & Environmental Sustainability, State University of New York at Binghamton, Binghamton, New York, 13902, USA

[†]Electronic supplementary information (ESI) available. See DOI: https://doi.org/ 10.1039/d4an00393d

Paper Analyst

natural settings.11 However, in vivo modeling is not practical because it requires labor-, skill-, and cost-intensive procedures and a relatively long time for biofilm formation. 17-19 Furthermore, the procedures provide little control of bacterial environments, biofilm thickness, and the formation of multispecies communities. 16 Meanwhile, in vitro models have been widely used because they are practical, cost-effective, and easily controlled.¹⁷ Although small deviations can occur in exactly mimicking the natural environment, in vitro models have become a powerful tool to understand biofilm formation and development. Moreover, they have fewer ethical concerns than those using living animals. 16 Closed static methods such as the calgary biofilm device (CBD) and the microtiter plate assay, and continuous dynamic approaches such as the flow cell system and the Centers for Disease Control (CDC) biofilm reactor are the most popular in vitro biofilm models. 16-19 The static models provide more cost-effective, less equipmentdependent, and more voluminous throughput while the dynamic models can mimic more in vivo-like bacterial communities with continuous introduction of nutrient and waste removal. However, existing static and dynamic in vitro models do not fully reflect the advantages of both technologies to meet the demands of a rapid and simple biofilm simulation concomitantly replicating the 3-D in vivo environments.

An innovative monitoring technique specific to biofilms is required to provide valuable information on the treatment efficacy against biofilm-related infections. 15 Rapid and highthroughput genotypic ASTs, which are widely used for planktonic bacteria, are quite limited for biofilm-forming bacteria because mechanisms of biofilm resistance are not fully understood and only a few resistant genes are known.²⁰ Moreover, genotypic AST methods require external bulky equipment, expensive reagents, and well-trained personnel.21 On the other hand, phenotypic ASTs have been widely adopted for biofilmbased infections²² while monitoring various phenotypic features such as growth, reproduction, motility, morphology, and physiology. 23,24 Among all phenotypic features, the gold standard ASTs (e.g., disk diffusion, gradient diffusion, and broth dilution) have been based on bacterial growth monitoring with antibiotics, which provide more reliable and direct information and generate a quantifiable minimum inhibitory concentration (MIC) of antibiotics for effective treatment of the infections. However, those culture-based approaches require a relatively long time for in vitro biofilm formation and assessment of the antibiotic effectiveness against thick biofilms.²⁵ The visual monitoring of bacterial growth and reproduction potentially requires at least overnight incubation and has limitations with non-culturable or slow-growing bacterial species. Furthermore, the methods cannot provide real-time monitoring of antibiotic efficacy nor early diagnosis of antibiotic resistance in biofilm. Although emerging single-cell growth monitoring in microfluidic channels is considered a promising alternative regarding turnaround time, reagent amount, and the needed space, 26,27 however, the technique is very limited to cells grown in planktonic form and cannot provide treatment guidance for biofilm-based infections.

Clinicians using our in vitro microbial biofilm model and innovative monitoring technique will be able to select the right antibiotics with the exact dose for the appropriate duration, which will revolutionize the effective treatment of biofilm-associated infections and slow the spread of antibiotic resistance. In this work, we create a powerful yet simple method to form a target biofilm and develop a combined electrical-electrochemical monitoring of the treatment efficacy against biofilm-based infections. This work allows clinicians to assess within about 2 hours whether an antibiotic will work against a biofilm-protected infection. That unprecedented speed is possible because a target biofilm can be formed from a low-volume bacterial culture within an hour and the rapid changes in the biofilm's electrical and electrochemical activities within about another hour indicate the effectiveness of the antibiotic. The proposed approach is based on a paper-based 3-D cell culture platform that recapitulates the structure, function, and physiology of bacterial biofilms and monitors bacterial metabolism rapidly and reliably by measuring microbial extracellular electron transfer (EET) and using electrochemical impedance spectroscopy (EIS) across a microbe-electrode interface (Fig. 1). Monitoring bacterial metabolism through the combined electrical-electrochemical technique allows an innovative phenotypic evaluation of the antibiotic effectiveness against the engineered biofilms and a detailed characterization of the antibiotic action mechanism, which is much faster and more sensitive than conventional growth-based ASTs.

2. Results and discussion

2.1 In vitro biofilm formation, development, and characterization

First, we developed in vitro biofilm model that can rapidly and simply represent the in vivo environment by using a paper-

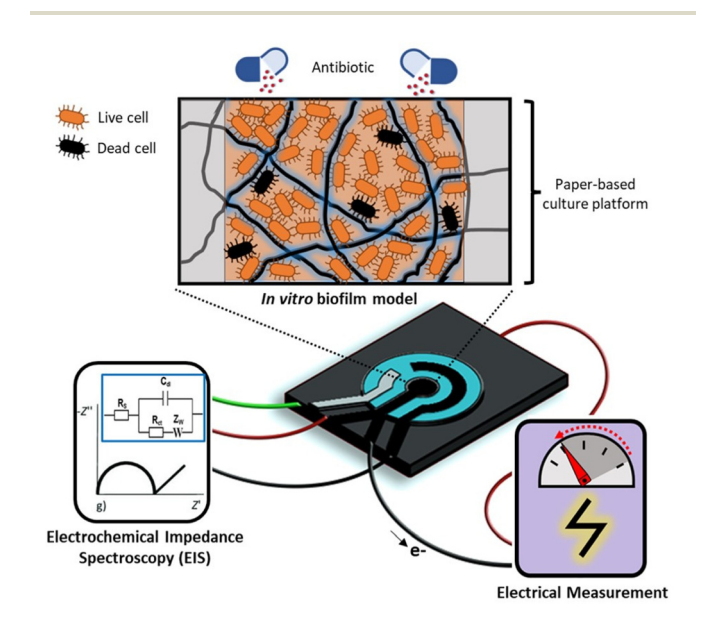


Fig. 1 A conceptual illustration of our proposed AST platform for in vitro biofilm models.

based cell culture platform. Paper-based cultures have been used to create 3-D tissue models to understand disease developments, drug screens, co-culture synergies, and molecular analyses.²⁸ Various paper-based models for liver tissue, cardiac disease, blood-brain barrier, Alzheimer's disease, cancer, tumor organoid, and bone tissue have been successfully demonstrated.²⁸⁻³⁵ Unfortunately, no other groups have used the paper-based technique for bacterial biofilm formation. Very recently, our group partially demonstrated that the paperbased platform can find the best-fit solution to form densely packed aggregates of bacterial cells.³⁶ We successfully created multispecies co-culture systems and controllable spatiotemporal gradients of oxygen, nutrients, and bacterial waste products. Despite excitement about these achievements, however, studies could not explore whether the cells cultured in paper are a simple bacterial aggregate in the planktonic phase or an actual physiologically defined biofilm that can represent a new in vitro model for biofilm formation and development.

A 10 µL volumetric hydrophilic chamber was defined and constructed by simply printing hydrophobic wax boundaries on a hydrophilic filter paper and heat-treating it for the wax penetration through the paper (Fig. 1a). For the electricalelectrochemical monitoring to be discussed in the next session, the chamber was engineered to be conductive by introducing water-soluble poly(3,4-ethylenedioxythiophene): poly(styrene sulfonate) (PEDOT:PSS).37 The PEDOT:PSS serves as a conductive polymer ink that tightly and uniformly coats the individual non-conductive paper fibers. ^{37–39} The treatment did not change the paper morphology and porosity, which provided a 3-D natural habitat for biofilm formation and efficient metabolic activities through the pores. Adding 3-glycidoxypropy-trimethoxysilane (3-GLYMO) converted the hydrophobic PEDOT:PSS coated paper surface to hydrophilic so that liquid bacterial samples could be readily and rapidly adsorbed via capillary force. The hydrophilic property allowed for instrument-free liquid transport and storage of biological and chemical reagents. The biocompatibility and the strong wicking force of the engineered paper improved cell adhesion in aquatic cultures and facilitated biofilm formation. Moreover, a porous, mechanically strong network of intertwined cellulose fibers in paper served as an excellent scaffold to recapitulate the 3-D cellular microenvironments. 40 At t =1 hour, 2 hours, and 5 hours after introducing Pseudomonas aeruginosa with ~109 CFU mL⁻¹ (corresponding to 1.0 OD₆₀₀ (optical density at 600 nm)), we assessed the biofilm formation and development by using fluorescence microscopy (Fig. 2b) and a scanning electron microscope (SEM) (Fig. 2c and Fig. S1a†). To minimize the nutrient loss through evaporation and depletion, we added 10 µL lysogeny broth (LB) every hour into the chamber. At t = 1 hour, a thin but seamless biofilm fully covered the paper-based chamber and became embedded in an extracellular polymeric substance (EPS). The strong capillary force rapidly pulls a large number of cells upward and with the aid of the EPS develops a multilayer biofilm. The accumulation ultimately peaks at 2 hours. At t = 5 hours, the SEM image shows very thick, uniform, and densely packed

biofilm on the entire surface. In addition to that image-based qualitative assessment of the biofilm, quantitative biofilm characterization was performed by using the well-established bicinchoninic acid (BCA) assay kit⁴¹ while the biofilm formed in our paper was compared to conventional static and dynamic models (Fig. 2d). Usually, biofilm can be characterized and quantified by proteins comprising a significant proportion of the EPS. 41 The BSA assay is based on the reduction of copper ions by the EPS proteins and their concentration is related to the degree of the reduction which exhibits a strong UV absorbance at 562 nm. The static and dynamic biofilm test setups were also prepared on the same paper-based culture platforms which were fully encapsulated by 100 µL volumetric microfluidic chambers. The microfluidic chamber has an inlet and an outlet for proper operation. To remove the effect of capillary wicking advantage on the biofilm formation, the paper-based culturing regions were fully saturated with LB media so that the biofilm formation can be driven by diffusion and gravity for the static mode, and fluid and shear stress for the dynamic mode. For the static and dynamic tests, the same bacterial concentration as our paper-based culturing setup was used in the 100 µL microfluidic chamber. The bacterial inoculum was continuously supplied using the syringe pump at a rate of 10 µL min⁻¹ for the dynamic mode while the static chamber was manually filled by the inoculum and sealed. Interestingly, a significant amount of the EPS proteins was measured from our paper-based culture platform even at t = 1 hour, which is a distinct indicator of biofilm development. At that time, any biofilm formation was not detected from the static test setup while a small concentration of the proteins was detected from the dynamic mode. At t = 2 hours, the static method started to form a decent biofilm but much more slowly than the dynamic and the paper-based culturing methods. At t =5 hours, the dynamic mode generated slightly more proteins than the paper platform, which indicates a little bit better biofilm function and health. This is because the dynamics of shear stress can promote biofilm development over time. 42 However, our paper-based platform developed a high-quality biofilm comparable to the dynamic one. Rather, given that the complicated fluidic operation and external equipment with fluidic tubes are required for the dynamic method, our paperbased culture platform can revolutionarily recapitulate the in vivo biofilm environment in a faster, more cost-effective, and less labor-intensive manner. Our paper-based culture platform allowed a biofilm formation of a mixed co-cultured sample (Escherichia coli and Pseudomonas aeruginosa) while two layers of paper containing each species were controllably stacked with a spatially structured network (Fig. S1b and S1c†). Both culturing platforms formed biofilms while each biofilm's development and quality varied according to the format (Fig. S2†). While further research into the dynamics of gene expression is essential for a more comprehensive understanding of biofilm formation, our observations unequivocally revealed an assembly of microbial cells firmly attached to a surface and encapsulated within an EPS matrix. Our simple, rapid, low-cost, equipment-free technique forms biofilms

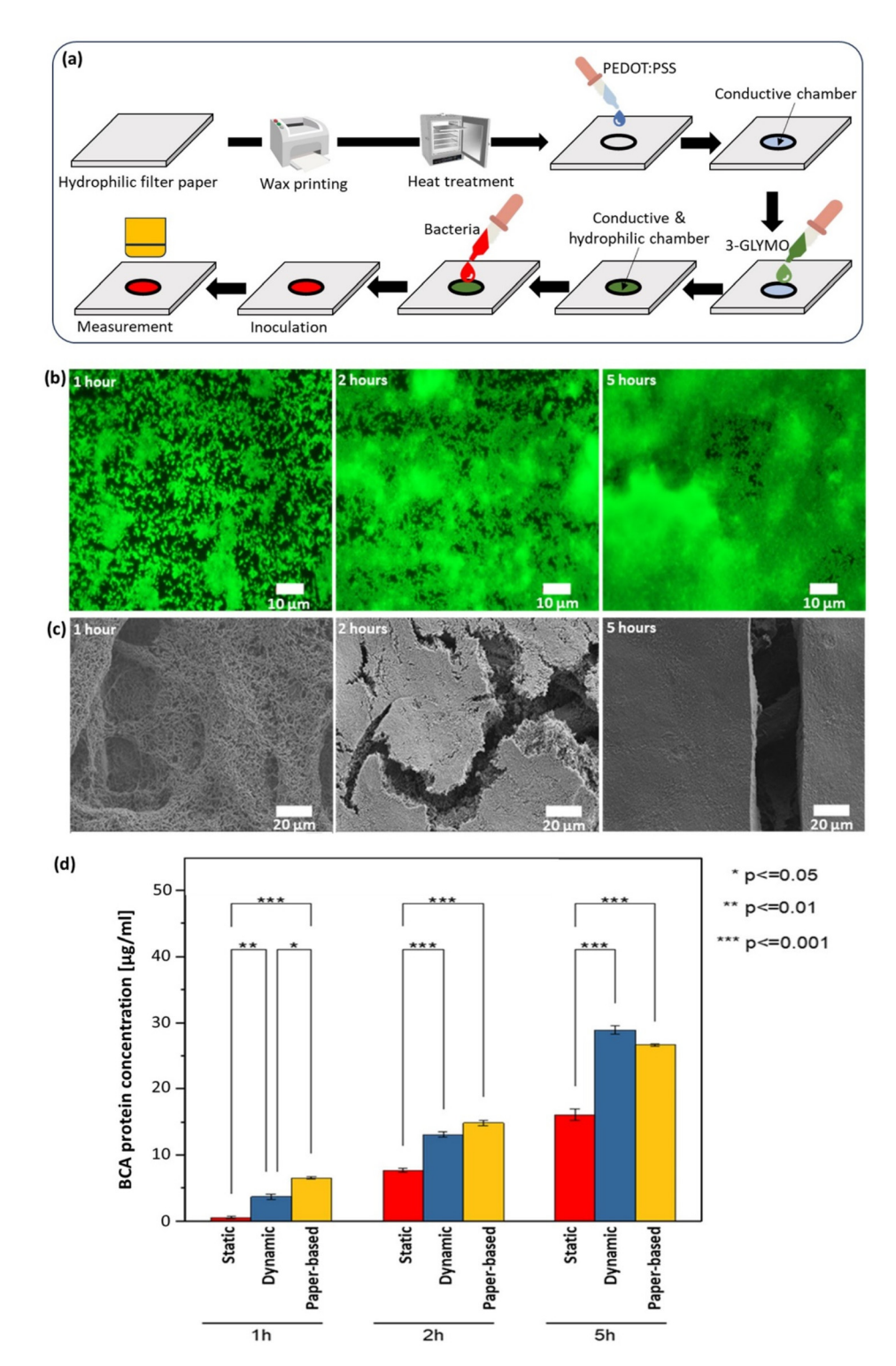


Fig. 2 (a) Fabrication overview of the paper-based culture platform, (b) Fluorescence microscopic images and (c) SEM images of *Pseudomonas aeruginosa* after 1 hour, 2 hours, and 5 hours inoculation within the patterned paper region. (d) Quantification of bacterial biofilm formation over time based on static, dynamic, and our paper-based culturing methods by using a BCA protein assay kit.

better than those created by the static model while it mimics the quality of the complex, diverse 3-D biofilms produced by the dynamic *in vitro* model. Additionally, simple paper cutting allowed easy follow-up studies in a non-destructive way without complicated extraction procedures of biofilms (Fig. 2d).

Analyst Paper

2.2 Combined electrical-electrochemical monitoring for antibiotic susceptibility profiling

Conventional phenotypic monitoring of the antibiotic effectiveness against the formed biofilm requires a time-consuming culture-based technique, adding to the delay required by the standard methods of forming biofilms. The monitoring requires visual inspections before and after antibiotic treatment to determine whether the biofilm has been inhibited. That is another long process that requires clinicians to wait until the actual number of cells noticeably changes in the presence of antibiotics. Recently, a bacterial metabolic perturbation has emerged as an indicator of antibiotic efficacy because bacterial metabolism plays an important role in reflecting their viability, growth, and reproduction, and antibiotics directly induce metabolic changes in biofilms. 43-46 Many reports demonstrated the interplay among action mechanisms of antibiotics, bacterial metabolism, and eventually their growth inhibition. 47,48 For the rapid phenotypic AST, such metabolic changes have recently been monitored by measuring redox interactions of labeled reporters which are involved in bacterial respiration, pH change, and enzyme production during bacterial metabolism. 46,49-51 Although those label-based metabolic sensing techniques are successful as a rapid and user-friendly AST approach, there is a growing interest in developing a label-free AST technique because of its overwhelming advantages including simplified steps, reduced amounts of reagents, point-of-care realization, and costeffectiveness. 45,52 For the label-free metabolic sensing, our group demonstrated that the electrons metabolically produced from Pseudomonas aeruginosa can be a strong signal to monitor their growth and treatment efficacy, successfully providing a quantifiable MIC of three antibiotics (i.e., gentamicin, ciprofloxacin, and ampicillin), and characterized the bacterial antibiotic action mechanisms. 53-55 A microbial fuel cell (MFC) was created as a metabolic biosensor where the anode incubated the pathogen with antibiotics. An effective antibiotic caused sufficient inhibition to the bacterial metabolisms, decreasing the extracellular electron transfer (EET) to the anode. Meanwhile, the metabolically produced protons traveled to the cathode through an ion exchange membrane while the electrons moved to the cathode through an external circuit. Although our technique enabled all-electrical, realtime, easy-to-use monitoring, it has not yet been successfully translated into commercial applications because the extremely small number of electrons produced from bacterial metabolic activities requires an additional strategy for signal amplification or signal accumulation,53,54 which will complicate the overall system design and operation and increase the cost. Moreover, some pathogens which are not capable of transferring electrons require additional electron mediators, increasing the number of steps and cost, and losing the advantage of a label-free approach.46

Here, we created a practical, reliable, and generalizable phenotypic monitoring technique by combining the MFC-based EET sensing technique and an electrochemical impedance

sensing technique. Previously, electrochemical impedance spectroscopy (EIS) has been used to investigate antibiotic susceptibility indirectly, but more conveniently, to monitor bacthan the conventional terial growth culture-based technique. 56,57 In particular, the bacterial metabolic perturbation can be rapidly probed by the impedance change at the microbe-electrode. 58-64 Usually, the impedance is determined by the dielectric properties at the interface, the resistance of the bulk electrolyte, and the electron transfer efficiencies, which are all sensitively affected by bacterial metabolic activities.65 Moreover, the bacterial cell body acts as an insulator while the internal components of the cells and the cellular metabolic byproducts are conductive. The presence of antibiotics can significantly change the whole impedance and various impedance parameters. Therefore, the integration of the impedance sensing technique with the MFC-based innovation will revolutionize the AST performance and practice as a rapid AST technique, especially for biofilm-based infections.

In this work, we created a combined MFC-EIS AST device for pathogenic biofilms. The low electrical signal from the MFC was significantly improved by the addition of gold nanoparticles (Au-NPs), which can create activation centers on anodic surfaces to improve biofilm formation and electron transfer efficiencies. Thus, the MFC's electrical signal does not need to be amplified or cumulatively added through an additional system or computational process. The combined MFC-EIS monitoring system was integrated into a two-layer paper-based device (Fig. 3). The conductive culture chamber in the middle of the top paper layer was prepared with the combination of the PEDOT:PSS and Au-NPs and was shared by the MFC as an anode and the EIS as a working electrode. For a three-electrode EIS configuration, a carbon-based counter and Ag/AgCl reference electrodes were precisely screen-printed on the top layer with defined dimensions. The second paper layer was first printed with the hydrophobic wax and then controllably heat-treated to ensure the wax penetrated the whole thickness of the paper.

That wax layer was used as an ion exchange membrane. Finally, the cathode was constructed with a mixture of PEDOT: PSS and Ag₂O. Ag₂O is widely used for power-producing devices as a cathodic catalyst because of its high efficiency and stability. 66,67 Three representative pathogens, Pseudomonas aeruginosa, Escherichia coli, and Staphylococcus aureus, were tested against three frontline antibiotics with different action modes (gentamicin, ciprofloxacin, and ceftazidime) (Fig. S3a†). Gramnegative P. aeruginosa is an opportunistic pathogen that can lead to serious and life-threatening infections.⁵⁴ Its wellknown EET capability is based on an indirect shuttle transfer mechanism through microbially-produced electron mediators. Therefore, its metabolic activities are expected to be monitored synergistically using the MFC and the EIS together. Gramnegative E. coli is one of the leading pathogens causing urinary tract, blood-stream, and many other infections in humans. Because E. coli is a well-known non-exoelectrogenic species, 68 the MFC with E. coli will not generate any meaningful electrical outputs while the EIS will be the main monitoring techPaper Analyst

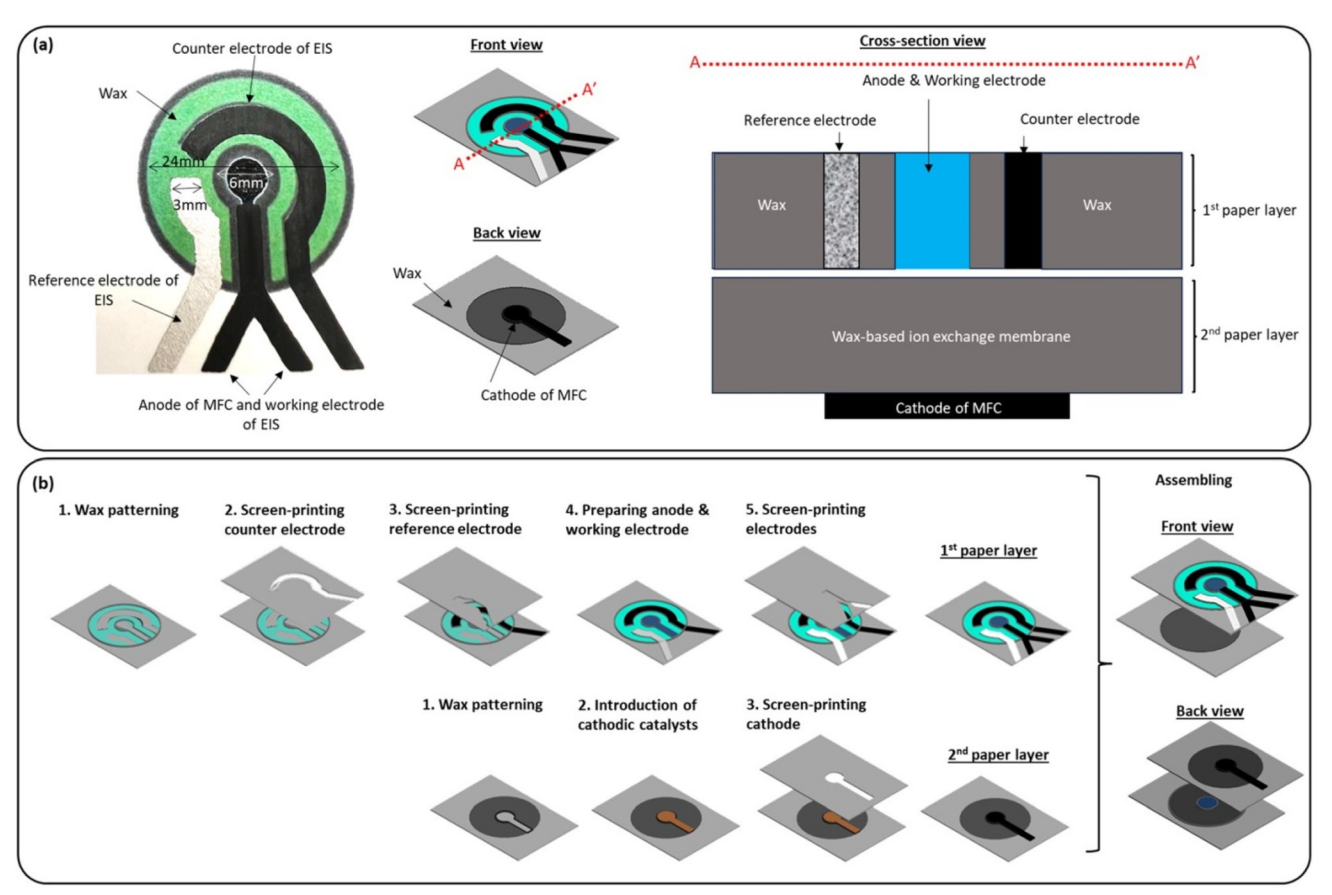


Fig. 3 Overview of the configuration and fabrication of the combined electrical-electrochemical AST device. (a) A picture of the assembled device and schematic diagrams of the front, back, and cross-section of the device. (b) Fabrication processes of the individual paper layers.

nique. Finally, Gram-positive Staphylococcus aureus is one of the most infectious pathogens, causing a wide range of clinical diseases.⁵⁹ This pathogen inhabits and thrives in the human body, secreting extracellular vesicles that can regulate bacterial resistance to antibiotics. Although the EET pathway of S. aureus is very complicated, S. aureus has a distinct electrogenic capability.⁶⁹ The MFC and EIS can be complementary to provide valuable phenotypic information for a quantitative understanding of antibiotic effectiveness and action mechanisms. Three different antibiotics represent three fundamentally different action mechanisms; gentamicin (GEN) inhibits protein synthesis by binding to a site on the 30S ribosome, ciprofloxacin (CIP) prevents DNA replication by inhibiting the activity of DNA gyrase, and ceftazidime (CEF) inhibits cell wall synthesis by adverting formation of peptidoglycan. 51 Antibiotic effectiveness, concentration, and action mechanism will change the magnitude of the MFC electricity and will differently affect individual impedance parameters.

First, the anodes (or working electrodes) were inoculated by individual bacterial species with a concentration of 1.0 OD₆₀₀ and were left for 1 hour to form their biofilms. Then, antibiotics with different concentrations were introduced. We waited for 1 hour to provide sufficient time for the bacteria to interact with antibiotics. The electrical currents harvested

from bacterial metabolism in the MFC were monitored through various external resistors and their corresponding power outputs were calculated. The current and power densities were normalized to the anode (or the working electrode) surface area (Fig. 3a). Once the electrical parameters were obtained from the MFC, the EIS measurements were performed using a potentiostat. 0.1 M KCl electrolyte was applied to cover all three electrodes on the top paper layer (Fig. S3b†). The EIS measures the reactance and resistance of the microbeelectrode interface in the electrolyte across a spectrum of AC frequencies. All comprehensive and collective electrochemical activities of bacteria with the electrode, the dielectric properties of the bacterial cell body, and the electroactive species produced from microbial metabolism and released from the cells after antibiotic treatment will all affect the impedance measurement (Fig. S3c†). The measurement is well fitted to the Randles equivalent circuit model having four impedance parameters: the solution resistance (R_s) , the double-layer capacitance $(C_{\rm dl})$, the charge transfer resistance $(R_{\rm ct})$, and the Warburg impedance (Z_w) (Fig. S3d†).⁶⁰ Because the Z_w is a diffusional impedance and is very small at high frequencies, $Z_{\rm w}$ will be neglected here.⁷⁰ The monitoring of the microbial metabolic activities with the antibiotics here will be limited to kinetic processes.

For a bacterial species with different concentrations of an antibiotic, the current-voltage (I-V) and current-power (I-P) curves were obtained by measuring the voltage drops at external resistors (no resistor, 470 k Ω , 250 k Ω , 162 k Ω , 100 k Ω , 71 $k\Omega$, 47 $k\Omega$, 32 $k\Omega$, 22 $k\Omega$, 15 $k\Omega$, 10 $k\Omega$, 2 $k\Omega$, 1.5 $k\Omega$, 0.45 $k\Omega$, and 0.35 k Ω), which were automatically and sequentially connected by solenoid operated relays.³⁸ The voltages were recorded by data acquisition and their corresponding current and power values were calculated according to Ohm's Law and the Power Law (Fig. S4†). All measurements for the MFC were efficiently completed within a brief span of 4 minutes. The process entailed a systematic assessment, allocating 15 seconds for each resistor, and included a preparatory period of 1 minute for voltage recovery before initiating the subsequent test sequence. Then, the EIS measurements were performed with an AC rms voltage of 10 mV between 1 Hz and 100 kHz, which required only 7 minutes (Fig. S5†). All AST processes from biofilm formation (1 hour), antibiotic accumulation and electrical-electrochemical measurements (11 minutes) for a bacterial species toward an antibiotic required only 2 hours and 11 minutes. As shown in Fig. 4 and 5, the maximum power density from the MFC measurement (Fig. S4 \dagger), the solution resistance (R_s), the double-layer capacitance $(C_{\rm dl})$, and the charge transfer resistance $(R_{\rm ct})$ from the EIS measurement (Fig. S5†) were extracted and referenced against an identical control sample with no antibiotics according to the following equation.

$$\Delta X = \frac{|X - X_0|}{X_0} \times 100 \tag{1}$$

where ΔX is the normalized absolute change of parameter, X is the measured value, and X_0 is the control without antibiotics.

The composite of the PEDOT:PSS and Au-NPs in this miniaturized device platform significantly improved a signal-tonoise ratio for the rapid and sensitive power assessment of pathogens (Fig. S6a†). The MFC power output for electricityproducing bacterial species such as P. aeruginosa and S. aureus was a strong signal for monitoring bacterial growth and antibiotic treatment efficacy (Fig. 4 and Fig. S4†). Interestingly,

even the non-exoelectrogen, E-coli, generated meaningful electrical outputs even though their magnitude was not significant enough compared to P. aeruginosa and S. aureus. This is because the PEDOT:PSS conformally coated on the individual paper fibers mediates bacterial EET indirectly.³⁸ Additionally, the Au-NPs provided a high surface-to-volume ratio and were more favorable for the enhancement of the electrocatalytic property of the PEDOT:PSS matrices (Fig. S6a†).⁷¹

The normalized absolute change of the maximum power density of all three pathogens was outstanding with the increasing concentration of all antibiotics. The change of P. aeruginosa was the highest against GEN while the change of E. coli against CIP and CEF was higher than P. aeruginosa and S. aureus. For GEN, the power output of all pathogens started to decrease significantly with 4 μg mL⁻¹ of GEN (Fig. S4† and Fig. 4a), which can be considered the minimum inhibitory concentration (MIC) (i.e., the lowest antibiotic concentration that can prevent the growth of a pathogen). The MIC values were comparable to those based on the Clinical and Laboratory Standards Institute (CLSI) guidelines (Table S1†). For CIP, E. coli and S. aureus demonstrated a significant power decrease with 0.5 µg mL⁻¹ of CIP while the power of P. aeruginosa showed a dominant change with its 1 µg mL⁻¹ (Fig. 4b). The MICs of CIP against S. aureus and P. aeruginosa are not in agreement with CLSI values (Table S1†). For CEF, the power value of all three pathogens started to have meaningful change with 4 μg mL⁻¹ of CEF (Fig. 4c), which generated a slight difference for P. aeruginosa and E. coli from the CLSI ones (Table S1†). That MIC discrepancy originated from the difference between the cells in the planktonic form (i.e., CLSI) and the 3-D biofilm. Their physiological and microenvironmental properties and thus treatment efficacy against antibiotics are expected to be different. Further studies are required to evaluate the effect of the increase in biofilm thickness on the treatment effectiveness. Although the MFC power value itself could provide the MIC information for the selected pathogenic biofilms, it was not sufficient as a signal to identify and characterize the antibiotic mechanism of action. Moreover, the error bars sometimes overlap, which demonstrates their statistical insignificance. Understanding the

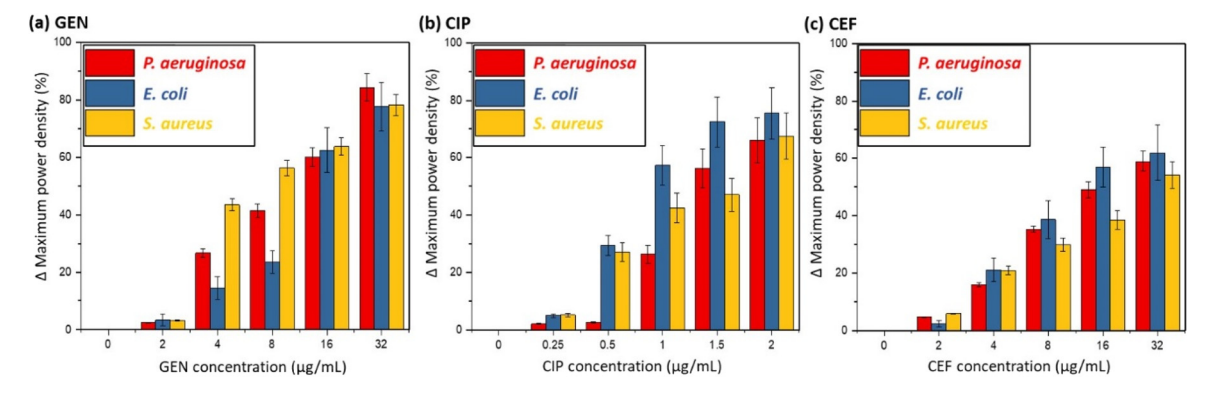
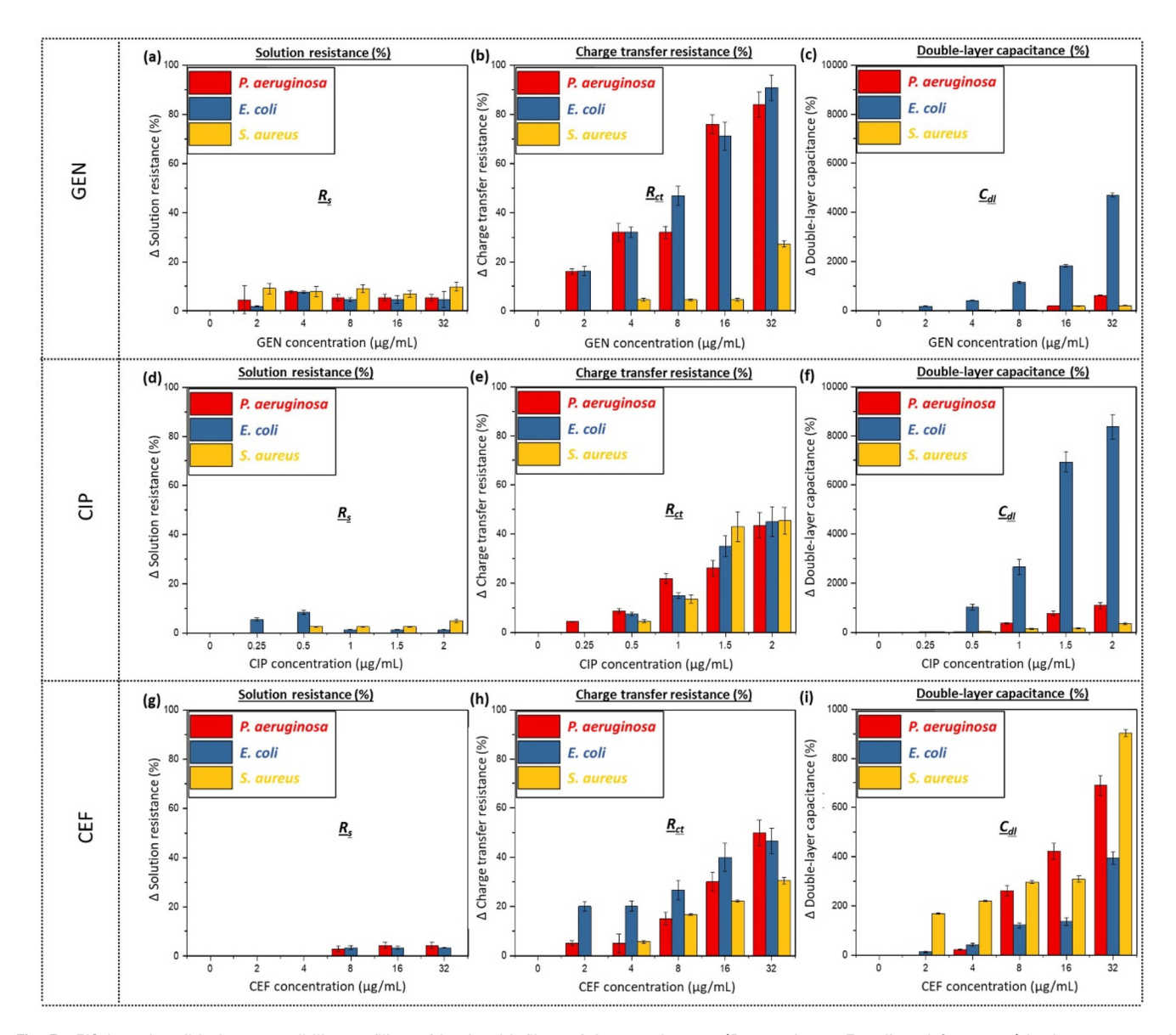


Fig. 4 MFC-based antibiotic susceptibility profiling of in vitro biofilms of three pathogens (P. aeruginosa, E. coli, and S. auresus) in the presence of three anbiotics; (a) GEN, (b) CIP, and (c) CEF. The normalized change of maximum power density is obtained.

Paper Analyst



action mechanism is critical to develop new antibiotics and provide more accurate MIC information.⁷²

Here, three impedance parameters, $R_{\rm s}$, $R_{\rm ct}$, and $C_{\rm dl}$, were obtained from the EIS measurement to eliminate the aforementioned major technical hurdles and provide a complementary technique to the MFC (Fig. 5 and Fig. S5†). Overall, the change in the $R_{\rm s}$ values for all three pathogens was negligible against all three antibiotics (Fig. 5). This means that the cell growth inhibition and cell death through whatever antibiotic action mechanisms did not affect the bulk properties of the electrolyte within that short time of the measurement. Theoretically, the inhibited protein synthesis through GEN

changes the permeability of the cell membrane⁷³ and the blocked penicillin-binding proteins through CEF inhibit the cell wall synthesis, ⁷⁴ which eventually leads to the release of ions to the electrolyte and changes its resistance over time. However, that time-consuming process was not detected with the $R_{\rm S}$ parameter.

GEN did not generate any meaningful data for the $R_{\rm s}$ (Fig. 5a). On the other hand, the $R_{\rm ct}$ of P. aeruginosa and E. coli against GEN started to significantly change with 2 μg mL⁻¹ of GEN while S. aureus did not show a dominant change until the GEN concentration increased to 32 μg mL⁻¹ (Fig. 5b). Given that the $R_{\rm ct}$ is determined by the kinetics of electron transfer

between bacteria and the electrode, 70 bacterial metabolic inhibition will decrease the R_{ct} while the release of electrochemical ions will increase the value oppositely. Therefore, measuring the overall change of the R_{ct} is critical to determine which component is the main dominator. Like the R_s parameter, the release of electrochemical ions did not show up within the short time through the Rct. The Rct decreases only with the increasing concentration of antibiotics, mainly being affected by metabolic activities. Meanwhile, the $C_{\rm dl}$ of P. aeruginosa and S. aureus did not change much while its value for E. coli significantly changed with the increasing GEN (Fig. 5c). Typically, the $C_{\rm dl}$ is formed at the microbe-electrode interface because of the charging/discharging behavior of (i) the biofilm, (ii) the individual cells, and (iii) the redox ions available.⁷⁰ Therefore, the comprehensive and collective capacitive responses of a pathogenic biofilm against an antibiotic will affect the $C_{\rm dl}$. Given that fact, GEN was more effective toward E. coli, converting electrochemical cells to dielectric dead cells within the short time of EIS measurement compared to P. aeruginosa and S. aureus.

For CIP, no $R_{\rm s}$ changes appeared (Fig. 5d). However, the $R_{\rm ct}$ was a more determinant parameter for S. aureus than GEN, showing that the inhibition of DNA replication through CIP against S. aureus can be better characterized (Fig. 5e). The absolute magnitude change of the $R_{\rm ct}$ for CIP against all pathogenic biofilms similarly increased. However, the change in the $C_{\rm dl}$ of E. coli was outstanding, followed by P. aeruginosa (Fig. 5f). No changes in the $C_{\rm dl}$ appeared with S. aureus.

For CEF, no R_s changes showed up (Fig. 5g). Meanwhile, the initial change in the Rct was noticeable from E. coli while its change of P. aeruginosa gradually increased and became the largest at 32 μ g mL⁻¹ of CEF (Fig. 5h). Although the R_{ct} change of S. aureus was smaller than the other two pathogens, its value increased with the increasing CEF concentration. S. aureus generated a significant change in the $C_{\rm dl}$ from the beginning which was much larger than that of P. aeruginosa and E. coli (Fig. 5i). Overall, each impedance parameter was selective for an action mechanism of antibiotics toward a specific pathogen. The $C_{\rm dl}$ can be a great parameter for E.~coliagainst GEN and CIP while the parameter is effective both for P. aeruginosa and S. aureus against CEF. The R_{ct} can be significantly useful for P. aeruginosa and E. coli against GEN. Those representative EIS parameters are in good agreement with the MIC values that were determined by the MFC measurement.

3. Conclusion

Bacterial infections from biofilms have emerged as a major threat to human health because bacteria in biofilms become very resistant to and tolerant of antibiotics and human immune responses. Effective and rapid antibiotic susceptibility testing (AST) for biofilms is urgently required to guide effective antibiotic use and to monitor the spread and emergence of antimicrobial resistance. This is by no means a simple challenge because it is extremely difficult to rapidly

develop standard models for the wide variety of biofilms, requiring a long time to assess antibiotic effectiveness against thick biofilms. Furthermore, all conventional and emerging AST techniques are based on homogeneous planktonic bacterial cells, leading to antibiotic treatment failure for biofilmbased infections. The overall objective of this work is to provide an innovative, practical, and reliable AST for pathogenic biofilms, which enables rapid (~2 hours), and real-time monitoring along with controllable manipulation of bacterial microenvironments and the rapid biofilm formation. Our approach monitors two complementary signals from bacterial extracellular electron transfers (EET) and electrochemical impedance changes at the microbe-electrode through their metabolic activities, which are impaired by effective antibiotics, thus decreasing the signals. The combined electricalelectrochemical outputs generated from the bacterial metabolism are sensitive enough to evaluate the antibiotic's effectiveness and characterize its action mechanism while readily providing all-electrical, real-time, and sensitive assessments. Furthermore, our novel strategy constructs rapidly a 3-D microbial biofilm, which establishes various biofilm models mimicking natural microbial microenvironments.

4. Materials and methods

4.1 Preparation of the paper-based culture platform

The boundary patterns were defined on a filter paper (Whatman 3 MM CHR) by printing the hydrophobic wax with a solid-ink printer (Xerox Phaser, ColorQube 8570) and penetrating the paper by heat treatment at 150° for 30 seconds. All wax patterns were designed using AutoCAD. The defined hydrophilic region within the boundaries was further treated with a mixture of 1 wt% PEDOT:PSS and 5 wt% dimethyl sulfoxide (DMSO) for conversion of non-conducting paper to conducting paper, which was used as an anode or a working electrode for the AST. The addition of DMSO improved the conductivity of PEDOT:PSS. Then, a 2 wt% 3-glycidoxypropy-trimethoxysilane (3-GLYMO) solution was added to the engineered paper region to increase its hydrophilicity. This engineered paper region served as a conductive, hydrophilic, and porous microbial culture reservoir, which had the same properties as the bare hydrophilic paper. Finally, 10 µL of P. aeruginosa with 1.0 OD₆₀₀ was inoculated in the engineered culture reservoir to form a biofilm. For static and dynamic biofilm models, 100 µL volumetric microfluidic chambers were constructed from a high-temperature resin by using a stereolithography-based 3D printer (Formlabs Form 3B). Then, the chamber was attached to the paper reservoir with an adhesive. One inlet and one outlet were integrated for bacterial sample loading and dynamic model operation. For the static model, the outlet was sealed after the sample was introduced.

4.2 Fluorescence imaging

To monitor the cell viability and biofilm formation, the paper reservoirs were submerged in phosphate-buffered saline and **Paper** Analyst

sonicated to harvest the cells. Under the fluorescence microscope, the live cells were identified with fluorescent dyes with carboxyfluorescein diacetate (cFDA).

4.3 Biofilm fixation and SEM imaging

The bacterial cells in the biofilm were fixed on the engineered cellulose fibers with 2.5% glutaraldehyde in 0.1 M phosphate buffered saline overnight. The fix samples were dehydrated by serial transfers through 35%, 50%, 75%, 95%, and 100% ethanol. Then, they were placed in a desiccator to dry overnight. After the samples were coated with carbon (208HR Turbo Sputter Coater, Cressington Scientific Instruments, UK), a field emission scanning electron microscope (FE-SEM, Supra 55 VP, Carl Zeiss AG, German) was used for examination.

4.4 BCA protein measurement

We followed the instruction of the Thermo Scientific Perce bicinchoninic acid (BCA) protein assay kit. This assay is based on the reduction of Cu2+ to Cu+1 by the EPS proteins in an alkaline medium. The Cu⁺¹ can be detected through a colorimetric reaction with the highly selective and sensitive BCA, which exhibits a strong UV absorbance at 562 nm. That absorbance is nearly linear with an increasing concentration of the EPS proteins.

4.5 Bacterial inoculum

P. aeruginosa, E. coli, and S. aureus were cultured in an LB medium with a pH of 7.0. The LB consisted of 10 g L⁻¹ tryptone, 5 g L⁻¹ NaCl, and 5 g L⁻¹ yeast, which were dissolved in 1000 mL of deionized (DI) water. Individual cultures were incubated at 37 °C for approximately 5, 8, and 6 hours, respectively, until they reached an optical density at 600 nm (OD₆₀₀) of 1.0, which corresponds to 10⁹ CFU ml⁻¹. Then, the cultures were centrifuged at 4000 rpm for 4 minutes. This centrifugation separated the bacterial cells from the supernatant. The supernatant was carefully discarded, and each cell pellet was subsequently resuspended in a fresh LB medium. This resuspension was achieved by subjecting the cell pellet to agitation using a vortex, ensuring thorough mixing of the cells with the new LB medium.

4.6 Preparation of antibiotics

One of each aminoglycoside, fluoroquinolones, and cephalosporins families that is gentamicin (GEN), ciprofloxacin (CIP), and ceftazidime (CEF), respectively, were selected as model antibiotics. GEN can interfere with protein synthesis and disrupt the outer membrane of pathogens. While CIP prevents DNA replication and stops their growth, CEF is known as a third-generation cephalosporin and usually inhibits the synthesis of the cell wall. A dilution series of GEN (0, 2, 4, 8, 16, & 32 μg mL⁻¹), CIP (0, 0.25, 0.5, 1, 1.5, & 2 μg mL⁻¹), and CEF (0, 2, 4, 8, 16, & 32 μg mL⁻¹) were prepared in sterile LB medium to obtain the MIC values against each pathogen.

4.7 Preparation of the combined electrical-electrochemical AST device

The electrochemical impedance spectroscopy (EIS) based three-electrode biosensor was constructed on the first top paper layer (Whatman 3MM CHR filter paper). A carbon-based (NC1114936, Fisher Scientific Co., LLC) working electrode was built upon the paper-based culture platform while a carbonbased counter electrode and an Ag/AgCl (NC1176443, Fisher Scientific Co., LLC) reference electrode were prepared by screen-printing the corresponding materials through the wellmicropatterned paper stencil. The microbial EET was measured by a microbial fuel cell (MFC) that was created by attaching the second bottom paper layer that integrates an ion exchange membrane and a cathode. The paper-based culture platform on the top layer was shared as an anode with the EIS. The MFC was formed by stacking the anode, ion exchange membrane, and cathode vertically. Wax was printed on the second layer and penetrated the entire paper thickness by heat treatment. On the bottom of the wax-pattered membrane, a mixture of 2 mL PEDOT:PSS and 100 mg Ag₂O was screenprinted as the cathodic catalyst. To improve the electrocatalytic activity of the EIS and EET efficiency of the MFC, the paperbased culture platform was updated by adding 5 wt% Au-NPs with 40 nm particle size. The addition of PEDOT:PSS and Au-NPs caused no morphological change in the paper fibers demonstrating their thin, tight, and conformal coating (Fig. S6b†).

4.8 Electrical characterizations

The microbial EET was characterized by monitoring the voltage drops across various external resistors. Each resistor electrically isolated from the microcontroller by relays was automatically connected every 1 minute for 15 seconds to the MFC for synchronous electrical measurement. The corresponding current and power densities according to the anode surface area were calculated by Ohm's Law and Power Law, respectively.

Electrochemical characterizations 4.9

EIS measurements were performed using a potentiostat (Squidstat Plus, Admiral Instruments) in a dropped 100 µL of 0.1 M KCl solution on the three-electrode system. The impedance data were obtained within only 7 minutes by applying an AC rms voltage of 10 mV between 1 Hz and 100 kHz. The produced Nyquist impedance plots were well fitted to the Randles' equivalent circuit model to extract the solution resistance (R_s) , the double-layer capacitance (C_{dl}) , and the charge transfer resistance (R_{ct}) .

4.10 Statistical analysis

Statistical significance was determined at a threshold level of p < 0.05 using a two-way ANOVA with Tukey's multiple comparisons test. All experimental data shown in this work were performed by repeating identical experiments at least three times.

Data were represented as the mean \pm standard errors of those experimental replicates.

Author contributions

Zahra Rafiee: investigation, methodology, formal analysis, and data curation; Maryam Rezaie: investigation; Seokheun Choi: conceptualization, supervision, project administration, funding acquisition, writing – original draft, and writing – review, editing, and finalizing.

Conflicts of interest

There are no conflicts to declare.

Acknowledgements

This work was supported by the National Science Foundation (CBET #2100757 and ECCS # 2246975).

References

- K. Sauer, P. Stoodley, D. M. Goeres, L. Hall-Stoodley, M. Burnølle, P. S. Stewart and T. Bjarnsholt, *Nat. Rev. Microbiol.*, 2022, 20, 608–620.
- 2 A. Zhao, J. Sun and Y. Liu, Front. Cell. Infect. Microbiol., 2023, 13, 1137947.
- 3 J. S. Madsen, S. J. Sørensen and M. Burmølle, *Curr. Opin. Microbiol.*, 2018, 42, 104–109.
- 4 V. Guéneau, R. Charron, V. Costache, A. Bridier and R. Briandet, *Spatial analysis of multispecies bacterial bio-films*. in Methods in Microbiology: Elsevier; 2023.
- 5 Y. Su, J. T. Yrastoraz, M. Matis, J. Cusick, S. Zhao, G. Wang and J. Xie, *Adv. Sci.*, 2022, 9, 2203291.
- 6 M. H. Muhammad, A. L. Idris, X. Fan, Y. Guo, Y. Yu, X. Jin, J. Qiu, X. Guan and T. Huang, *Front. Microbiol.*, 2020, **11**, 928.
- 7 S. Galié, C. Garcia-Gutiérrez, E. M. Miguélez, C. J. Villar and F. Lombó, *Front. Microbiol.*, 2018, **9**, 898.
- 8 S. Joshi, D. Lahiri and R. R. Ray, *Microbial Biofilms: Challenges and Advances in Metabolomic Study*, Elsevier, 1st edn, 2020, p. 396.
- C. W. Hall and T. Mah, FEMS Microbiol. Rev., 2017, 41, 276–301.
- 10 M. D. Macià, E. Rojo-Molinero and A. Oliver, *Clin. Microbiol. Infect.*, 2014, **20**, 981–990.
- 11 T. Bjarnsholt, M. Alhede, M. Alhede, S. R. Eickhardt-Sorensen, C. Moser, M. Kuhl, P. O. Jensen and N. Hoiby, *Trends Microbiol.*, 2013, **21**, 466.
- 12 A. Penesyan, I. T. Paulsen, M. R. Gillings, S. Kjelleberg and M. J. Manefield, *Front. Microbiol.*, 2020, **11**, 2109.

- 13 P. Jorge, A. P. Magalhães, T. Grainha, D. Alves, A. M. Sousa, S. P. Lopes and M. O. Pereira, *FEMS Microbiol. Ecol.*, 2019, 95, fiz115.
- 14 H. K. N. Vyas, B. Xia and A. Mai-Prochnow, *Biofilm*, 2022, 4, 100069.
- 15 M. Jamal, W. Ahmad, S. Andleeb, F. Jalil, M. Imran, M. A. Nawaz, T. Hussain, M. Ali, M. Rafiq, M. A. Kamil and J. Chin, Med. Assoc., 2018, 81, 7–11.
- 16 I. Guzmán-Soto, C. McTiernan, M. Gonzalez-Gomez, A. Ross, K. Gupta, E. J. Suuronen, T. Mah, M. Griffith and E. I. Alarcon, *iScience*, 2021, 24, 102443.
- 17 G. Crivello, L. Fracchia, G. Ciardelli, M. Boffito and C. Mattu, *Nanomaterials*, 2023, **13**, 904.
- 18 N. Blanco-Cabra, M. J. LóPez-Martinez, B. V. Arévalo-Jaimes, M. T. Martin-Gómez, J. Samitier and E. Torrents, npj Biofilms Microbiomes, 2021, 7, 62.
- 19 K. Sung, M. Park, J. Chon and S. Khan, *Encycl. Infect. Immun.*, 2022, 4, 408–429.
- 20 M. Müsken, k. Klimmek, A. Sauer-Heiborn, M. Donnert, L. Sedlacek, S. Suerbaum and S. Häussler, npj Biofilms Microbiomes, 2017, 3, 22.
- 21 A. van Belkum, C. D. Burnham, J. W. A. Rossen, F. Mallard, O. Rochas and W. M. Dunne Jr., *Nat. Rev. Microbiol.*, 2020, 18, 299–311.
- 22 M. J. Franklin, C. Chang, T. Akiyama and B. Bothner, *Microbiol. Spectrum*, 2015, 3(10), 1128.
- 23 D. J. Shin, N. Andini, K. Hsieh, S. Yang and T. Wang, *Annu. Rev. Anal. Chem.*, 2019, 12, 41–67.
- 24 R. K. Shanmugakani, B. Srinivasan, M. J. Glesby, L. F. Westblade, W. B. Cardenas, T. Raj, D. Erickson and S. Mehta, *Lab Chip*, 2020, 20, 2607–2625.
- 25 B. Behera, A. Vishnu, S. Chatterjee, V. S. N. Sitaramgupta, N. Sreekumar, A. Nagabhushan, N. Rajendran, B. H. Prathik and H. J. Panday, *Biosens. Bioelectron.*, 2019, 142, 111552.
- 26 Y. Yang, K. Gupta and K. L. Ekinci, *Proc. Natl. Acad. Sci. U. S. A.*, 2020, 117, 106396–110644.
- 27 K. Zhang, S. Qin, S. Wu, Y. Liang and J. Li, *Chem. Sci.*, 2020, **11**, 6352–6361.
- 28 D. Lantigua, Y. N. Kelly, B. Unal and G. Camci-Unal, *Adv. Healthcare Mater.*, 2017, **6**, 1700619.
- 29 B. Mosadegh, B. E. Dabiri, M. R. Lockett, R. Derda, P. Campbell, K. K. Parker and G. M. Whitesides, Adv. Healthcare Mater., 2014, 3, 1036.
- 30 Y. Wang, W. Su, L. Wang, L. Jiang, Y. Liu, L. Hui and J. Qin, *Toxicol. Res.*, 2018, 7, 13.
- 31 K. Huang, A. D. Castiaux, R. Podicheti, D. B. Rusch, R. S. Martin and L. A. Baker, *Small Methods*, 2021, 5, 2100592.
- 32 N. A. Whitman, Z. Lin, T. J. DiProspero, J. C. McIntosh and M. R. Lockett, *Anal. Chem.*, 2018, **90**, 11981.
- 33 X. Wu, K. Walsh, S. Suvarnapathaki, D. Lantigua, C. McCarthy and G. Camci-Unal, *Biotechnol. Bioeng.*, 2021, 118, 1411.
- 34 T. S. Larson, G. L. Glish and M. R. Lockett, *Anal. Chim. Acta*, 2021, **1186**, 339091.

- 35 M. Liu, H. Liu, S. Li, Y. Zhong, Y. Chen, Z. Guo, W. Chen, X. Lin, Y. Lei and A. Liu, *Talanta*, 2021, 223, 121738.
- 36 A. Elhadad and S. Choi, Analyst, 2022, 147, 4082-4091.
- 37 Y. Gao and S. Choi, Adv. Mater. Technol., 2018, 3, 1800118.
- 38 M. Tahernia, M. Mohammadifar, Y. Gao, W. Panmanee, D. J. Hassett and S. Choi, *Biosens. Bioelectron.*, 2020, **162**, 112259.
- 39 M. M. Hamedi, A. Ainla, F. Guder, D. C. Christodouleas, M. Fernandez-Abedul and G. M. Whitesides, *Adv. Mater.*, 2016, 28, 5054–5063.
- 40 M. Tahernia, M. Mohammadifar and S. Choi, *Micromachines*, 2020, **11**, 99.
- 41 C. Wilson, R. Lukowicz, S. Merchant, H. Valquier-Flynn, J. Caballero, J. Sandoval, M. Okuom, C. Huber, T. D. Brooks, E. Wilson, B. Clement, C. D. Wentworth and A. E. Holmes, Res. Rev.: J. Eng. Technol., 2017, 6, 4.
- 42 E. Tsagkari, S. Connelly, Z. Liu, A. McBride and W. T. Sloan, *npj Biofilms Microbiomes*, 2022, **8**, 33.
- 43 G. Pitruzzello, S. Johnson and T. F. Krauss, *Biosens. Bioelectron.*, 2023, 224, 115056.
- 44 S. Hannah, R. Doming-Roca, P. A. Hoskisson, M. E. Murphy and D. K. Corrigan, *Curr. Opin. Electrochem.*, 2022, 35, 101033.
- 45 C. Toyos-Rodriguez, D. Valero-Calvo and A. de la Escosura-Muñiz, *Anal. Bioanal. Chem.*, 2023, 415, 1107–1121.
- 46 G. Tibbits, A. Mohamed, D. R. Call and H. Beyenal, *Biosens. Bioelectron.*, 2022, **197**, 113754.
- 47 J. M. Stokes, A. J. Lopatkin, M. A. Lobritz and J. J. Collins, *Cell Metab.*, 2019, **30**, 251–259.
- 48 P. Belenky, J. D. Ye, C. B. M. Porter, N. R. Cohen, M. A. Lobritz, T. Ferrante, S. Jain, B. J. Korry, E. G. Schwarz, G. C. Walker and J. J. Collins, *Cell Rep.*, 2015, 13, 968–980.
- 49 X. Xu, S. Chen, Y. Yu, P. Virtanen, J. Wu, Q. Hu, S. Koskiniemi and Z. Zhang, *Sens. Actuators*, *B*, 2022, 357, 131458.
- 50 Y. Liu, T. Lehnert, T. Mayr and M. A. M. Gijs, *Lab Chip*, 2021, 21, 3520–3531.
- 51 D. Spencer, Y. Li, Y. Zhu, J. M. Sutton and H. Morgan, *ACS Sens.*, 2023, **8**, 1101–1108.
- 52 F. Abbasian, D. Golemi-Kotra, S. Magierowski and E. Ghafar-Zadeh, Label-free impedometric antibiogram test. 2019 IEEE 6th Portuguese Meeting on Bioengineering (ENBENG), DOI: 10.1109/ENBENG.2019.8692446.
- 53 Y. Gao, J. Ryu, L. Liu and S. Choi, *Biosens. Bioelectron.*, 2020, **168**, 112518.
- 54 Z. Rafiee, M. Rezaie and S. Choi, *Biosens. Bioelectron.*, 2022, 216, 114604.
- 55 Z. Rafiee and S. Choi, Analyst, 2023, 148, 2501-2510.

- 56 P. Swami, A. Sharma, S. Anand and S. Gupta, *Biosens. Bioelectron.*, 2021, **182**, 113190.
- 57 J. H. Song, S. Lee, I. H. Park, D. Yong, K. Lee, J. Shin and K. Yoo, *Biosens. Bioelectron.*, 2019, **143**, 111623.
- 58 M. Safavieh, H. J. Pandya, M. Venkataraman, P. Thirumalaraju, M. K. Kanakasabapathy, A. Singh, D. Prabhakar, M. K. Chug and H. Shafiee, ACS Appl. Mater. Interfaces, 2017, 9, 12832–12840.
- 59 A. C. Ward, A. J. Hannah, S. L. Kendrick, N. P. Tuccker, G. MacGregor and P. Connolly, *Biosens. Bioelectron.*, 2018, 110, 65–70.
- 60 S. Hannah, E. Addington, D. Alcorn, W. Shu, P. A. Koskisson and D. K. Corrigan, *Biosens. Bioelectron.*, 2019, 145, 111696.
- 61 R. Domingo-Roca, P. Lasserre, L. Riordan, A. R. Macdonald, A. Dobrea, K. R. Duncan, S. Hannah, M. Murphy, P. A. Hoskisson and D. K. Corrigan, *Biosens. Bioelectron.*: X, 2023, 13, 100308.
- 62 D. Butler, N. Goel, L. Goodnight, S. Tadigadapa and A. Ebrahimi, *Biosens. Bioelectron.*, 2019, **129**, 269–276.
- 63 P. Swami, G. Verma, A. Holani, S. Kamaraju, V. Manchanda, V. Sritharan and S. Gupta, *Biosens. Bioelectron.*, 2022, 200, 113876.
- 64 D. C. Spencer, T. F. Paton, K. T. Mulroney, T. J. J. Inglis, J. M. Sutton and H. Morgan, *Nat. Commun.*, 2020, **11**, 5328.
- 65 A. C. Ward, P. Connolly and N. P. Tucker, *PLoS One*, 2014, 14, e91732.
- 66 K. Zuo, H. Liu, Q. Zhang, P. Liang, X. Huang and C. D. Vecitis, *ChemSusChem*, 2015, 8, 2035–2040.
- 67 X. Xie, M. Ye, P.-C. Hsu, N. Liu, C. S. Criddle and Y. Cui, Proc. Natl. Acad. Sci. U. S. A., 2013, 110, 15925–15930.
- 68 O. Simoska, D. A. Cummings Jr., E. M. Gaffney, C. Langue, T. G. Primo, C. J. Weber, C. E. Witt and S. D. Minteer, ACS Sustainable Chem. Eng., 2023, 11, 11855–11866.
- 69 M. Tahernia, E. Plotkin-Kaye, M. Mohammadifar, Y. Gao, M. Oefelein, L. Cook and S. Choi, ACS Omega, 2020, 5, 29439–29446.
- 70 S. Brosel-Oliu, N. Abramova, N. Uria and A. Bratov, *Anal. Chim. Acta*, 2019, **1088**, 1–19.
- 71 L. Liu and S. Choi, J. Power Sources, 2021, 506, 230251.
- 72 M. A. Hudson and S. W. Lockless, *mBio*, 2022, **13**, 02240–02221.
- 73 M. Mingeot-Leclercq, Y. Glupczynski and P. M. Tulkens, *Antimicrob. Agents Chemother.*, 1999, **43**, 727.
- 74 J. F. Mosley, L. L. Smith, C. K. Parke, J. A. Brown, A. L. Wilson and L. V. Gibbs, *Pharm. Ther.*, 2016, 41, 479– 483.